



Archeological wood conservation with selected organosilicon compounds studied by XFM and nanoindentation

Magdalena Broda¹ · Joseph E. Jakes² · Luxi Li³ · Olga A. Antipova³

Received: 25 April 2023 / Accepted: 28 September 2023 / Published online: 11 October 2023
© The Author(s) 2023

Abstract

Waterlogged wood conservation is a complex and challenging task. Detailed knowledge about the interactions between the applied chemicals and wood is necessary to ensure the effective and safe conservation of wooden artifacts. The present research aims to determine the mechanism of dimensional stabilization of archeological wood by organosilicon compounds using the combination of synchrotron-based X-ray fluorescence microscopy (XFM) and nanoindentation. Archeological oak wood was treated with methyltrimethoxysilane, (3-mercaptopropyl)trimethoxysilane, or 1,3-bis-[(diethylamino)-3-(propoxy)propan-2-ol]-1,1,3,3-tetramethyldisiloxane, which in previous studies were found to be more effective than other organosilicons in stabilizing wood dimensions. The XFM and nanoindentation results showed that all three organosilicons infiltrated wood cell walls and enhanced their mechanical properties. The XFM also showed that part of the chemicals filled some void spaces like cell lumina. Based on the results obtained here and in our previous research, it is determined that the mechanism of archeological wood dimensional stabilization by organosilicon treatment is complex and likely involves both filling cell lumina and infiltration into cell walls where organosilicons interact with wood polymers.

✉ Magdalena Broda
magdalena.broda@up.poznan.pl

¹ Department of Wood Science and Thermal Techniques, Faculty of Forestry and Wood Technology, Poznan University of Life Sciences, ul. Wojska Polskiego 38/42, 60-637 Poznan, Poland

² Forest Biopolymers Science and Engineering, USDA Forest Service, Forest Products Laboratory, One Gifford Pinchot Drive, Madison, WI 53726, USA

³ X-ray Science Division, Advanced Photon Source, Argonne National Laboratory, 9700 S. Cass Avenue, Lemont, IL 60439, USA

Introduction

Waterlogged wooden artifacts found in water bodies or wet soil require immediate and appropriate conservation treatment directly after excavation to preserve their appearance and dimensions. “Waterlogged” refers to the state where all pore spaces in wood tissue are entirely filled with water. It is known that the mechanical properties of even visually intact waterlogged wood cell walls are deteriorated to some extent due to degradation of the main wood polymers over time (Han et al. 2020). When such wood is exposed to air, it starts drying uncontrollably, which may result in its cracking, distortions, or even complete disintegration as a consequence of shrinkage and collapse due to drying stresses and capillary tension of evaporating water (Grattan 1987; Kaye 1995). Various consolidants have been used in conservation practice to prevent this and provide integrity and dimensional stabilization upon drying, e.g., alum, polyethylene glycols (PEGs), or different sugars (Unger et al. 2001; Broda and Hill 2021). Because each of them has some drawbacks, extensive research has been undertaken to find new, more reliable conservation agents for waterlogged wood (Broda and Hill 2021). Some of the newly tested approaches include the application of chitosan and its derivatives (Christensen et al. 2015; Walsh-Korb et al. 2022), lignin and its derivatives (McHale et al. 2016, 2017), cellulose and its derivatives (Antonelli et al. 2020; Wakefield et al. 2020), oligoamides (Papacchini et al. 2019), and halloysite nanotubes (Cavallaro et al. 2017; Parisi et al. 2020; Lisuzzo et al. 2021).

In our research, several organosilicon compounds were tested as waterlogged wood consolidants, and some of them, including methyltrimethoxysilane, (3-mercaptopropyl)trimethoxysilane, and 1,3-bis-[(diethylamino)-3-(propoxy)propan-2-ol]-1,1,3,3-tetramethyldisiloxane, provided good dimensional stabilization during drying (Broda et al. 2019c, 2020; Broda and Yelle 2022). We already know that the selected compounds stabilize wood dimensions (Kowalczuk et al. 2019; Broda et al. 2020; Broda and Yelle 2022) and react with wood polymers (Popescu and Broda 2021; Broda and Yelle 2022). In addition, they reduce wood hygroscopicity and porosity but also have a plasticizing effect on wood (Broda et al. 2019a, 2021), are relatively resistant to leaching (Broda 2018; Broda et al. 2020), and provide wood with partial resistance to fungal decay (Broda 2018; Broda and Plaza 2023).

However, the mechanisms behind the stabilizing effect of these chemicals on the wood are still not fully recognized, and it remains unclear whether it includes the reinforcement of cell walls and restoration of their mechanical strength. In addition, the complex, multiscale structure of wood tissue makes it challenging to study. For example, consolidants may only flow into the micrometer-scale voids, such as lumina and pits, or they may also infiltrate into the cell wall materials. Norimoto cell wall modification models (Fig. 1) aid the discussion of the different types of interactions that can occur between consolidants and wood. For example, PEGs are known to completely fill cell lumina and also infiltrate cell walls (Hoffmann et al. 2004; Vorobyev et al. 2017), which would be Norimoto model A5. To better identify Norimoto cell wall modification models and understand the

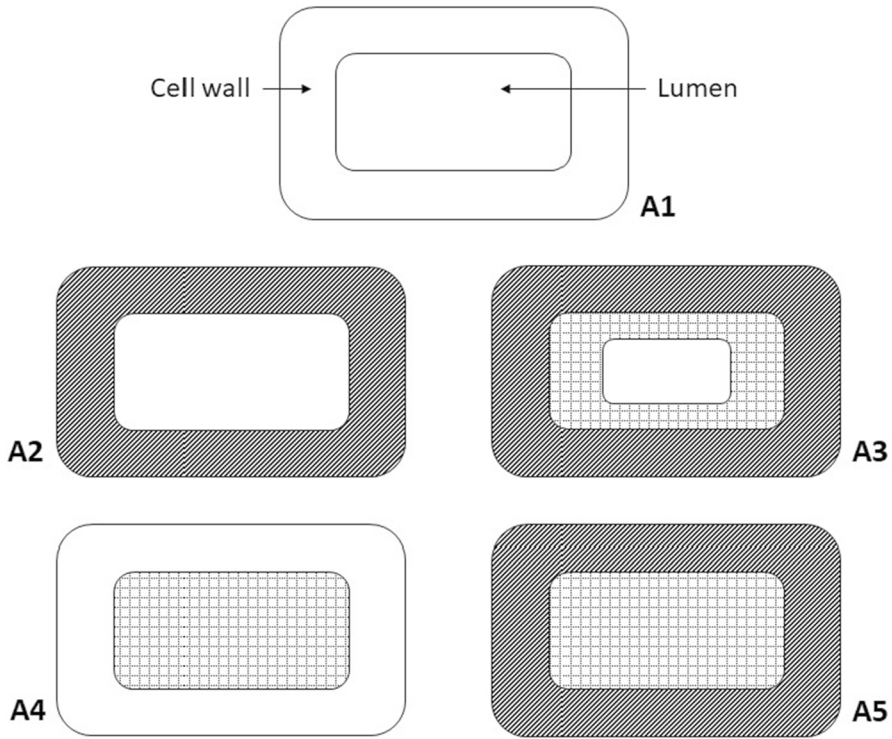


Fig. 1 Norimoto cell wall modification models, where A1 presents an unmodified wood cell, A2 shows infiltration of the cell wall by chemicals, A3 shows chemicals infiltrating the cell wall and partially filling the cell lumen, A4 shows chemicals filling only the lumen, and A5 shows chemicals both infiltrating the cell wall and completely filling the lumen (Norimoto 2001)

stabilization mechanisms for organosilicons, we decided to use synchrotron-based X-ray fluorescence microscopy (XFM) in conjunction with the nanoindentation technique to investigate the penetration of the organosilicons into the wood structure and assess their effect on the cell wall mechanical properties (Jakes et al. 2015).

Several methods enable the characterization of the wood structure, chemical composition, and mechanical properties at different scale levels. They include scanning electron microscopy (SEM) and other microscopy techniques, along with porosimetry, thermoporometry and N_2 nitrogen absorption methods useful for investigation of the wood structural features (Guo et al. 2019, 2022; Han et al. 2020; Balzano et al. 2022), scattering methods to characterize the wood structure at micro- and nanoscale along with characterization of cellulose crystallinity (Svedström et al. 2012; Han et al. 2020), wet chemical analysis, NMR techniques, Raman and Fourier-transform infrared spectroscopy and imaging for chemical analyses (Xia et al. 2018; Zhou et al. 2019; Han et al. 2020), as well as Dynamic Mechanical Analysis (DMA) and nanoindentation with or without embedding (Pizzo et al. 2018; Han et al. 2020; Broda et al. 2021) to

study the wood mechanics. However, studies directly relating the amount of cell wall infiltration to cell wall properties are lacking.

In our study, we aim to more fully understand the mode of action of organosilicon compounds on waterlogged archeological wood by studying the relationship between organosilicon infiltration into the cell wall and cell wall mechanics. Cell wall infiltration was studied using XFM and cell wall mechanics were studied using nanoindentation. XFM is characterized by high spatial resolution and sensitivity that allows simultaneous mapping and quantification of trace amounts of medium- to high-Z elements (e.g., Si atoms) (Paunesku et al. 2006). Using an X-ray beam focused on sub-micrometer spot size, XFM has proven valuable for mapping mineral ions and labeled organic molecules in individual wood cell wall layers (Jakes et al. 2015, 2020; Kirker et al. 2017). Because organosilicons contain Si, the Si XFM maps were used to map and quantify organosilicon compounds within the treated wood cell walls and cell lumina, which is impossible using other chemical analyses.

Nanoindentation is a technique for measuring material mechanical properties at a micrometer length scale, which is well suited to probe the mechanical properties of individual wood cell walls (Wimmer et al. 1997). In the case of chemically modified wood, nanoindentation is an effective tool to assess the effect of the applied chemical infiltration on the mechanical properties of the cell wall (Jakes et al. 2015; Jakes and Stone 2021). It seems to be particularly useful for the investigation of mechanical properties of degraded wood (including archeological wood) due to the fact that larger-scale techniques, such as DMA, do not allow for obtaining precise results for the collapsed cellular structure with internal cracks (Spear and Broda 2020; Broda et al. 2022). Observed changes in cell wall mechanical properties will help to indicate if organosilicons infiltrate the cell walls and help identify Norimoto cell wall modification models. Additionally, measured mechanical properties will aid the understanding of how cell wall modifications affect mechanical properties and are related to dimensional wood stabilization by organosilicon compounds.

The present research aims to determine the mechanism of dimensional stabilization of waterlogged archeological wood by organosilicon compounds using the combination of synchrotron-based X-ray fluorescence microscopy and nanoindentation. This knowledge is crucial for applying these chemicals in conservation practice as an alternative to the unreliable existing solutions and will help develop novel materials for conserving valuable artifacts of wooden cultural heritage. Moreover, increasing knowledge of the interactions of organosilicon compounds with wood polymers and their influence on wood properties should accelerate the development of new adhesive systems for the wood industry, allowing replacement of the currently used formaldehyde-based adhesives and producing new advanced environmentally friendly wood-based materials and composites for industrial and residential applications. The results of the study could therefore be useful not only for wood conservators but also for the worldwide wood industry.

Materials and methods

Materials

Research material was archeological oak wood (*Quercus robur* L.) dating back to the tenth century, excavated from the soil in the basement of the Psalteria building at Ostrow Tumski (Cathedral Island) in Poznan (the Wielkopolska Region, Poland). The oak log used in the study, 15.5 cm in diameter, contained only heartwood and was relatively well preserved, with a loss of wood substance of about 10% (Broda and Popescu 2019). It was one of the construction elements of wooden fortifications (city walls) encircling the medieval early Piast settlement (Stempin 2018).

Small cubical samples with dimensions 20×20×10 mm (radial×tangential×longitudinal direction) were cut from the middle layer of the oak log, stretching from about 1.5 cm from the surface to 1.5 cm to the pith. This way, all the samples were at relatively similar levels of degradation.

Methods

Wood treatment with organosilicon compounds

Before treatment, archeological oak samples were first dehydrated in 96% ethanol for four weeks. Water promotes hydrolysis and condensation of organosilicon monomers (Osterholtz and Pohl 1992); therefore, water removal prevents preterm polymerization of organosilicon monomers in subsurface wood layers and facilitates their better diffusion deep into the wood structure, thus ensuring more even treatment throughout a whole wooden block.

Based on the results of our previous research, three organosilicon compounds effective in stabilizing wood dimensions were selected for archeological oak treatment, including Methyltrimethoxysilane (MTMS), (3-Mercaptopropyl)trimethoxysilane (MPTMS), and 1,3-Bis-[(diethylamino)-3-(propoxy)propan-2-ol]-1,1,3,3-tetra-methylidisiloxane (DEAPTMDs) (Broda et al. 2020). Wood impregnation with 50% organosilicon solutions in 96% ethanol was conducted according to the previously described procedure using the oscillating vacuum-pressure method to expedite the organosilicon diffusion into wood (Broda et al. 2020). Ten samples per treatment with each chemical were used, and ten samples remained untreated and served as a control.

After treatment, oak specimens were removed from impregnation solutions (control samples were removed from ethanol) and slowly air-dried in the fume hood at room temperature (21 ± 3 °C) and relative air humidity of $45 \pm 5\%$ for four weeks. Bulk density (ρ) was calculated as the ratio of the sample weight to sample volume after conditioning to ambient temperature and relative humidity.

Five replicates of each type were then oven-dried at 60 °C to a constant weight to obtain their dry mass necessary for bulk wood weight percent gain (WPG_{BW}) calculations to assess the amount of impregnation. WPG_{BW} was calculated based on

Eq. (1), where W_0 was an estimated oven-dry mass of the specimen before treatment (based on oven-dry masses of untreated control samples), and W_1 was the mass of a treated specimen oven-dried at 60 °C:

$$\text{WPG}_{\text{BW}} = \frac{W_1 - W_0}{W_0} \times 100 \quad (1)$$

The five remaining specimens of each type were measured in three anatomical directions (3 measurements in each direction per sample) with a digital caliper (± 0.01 mm) to calculate the volumetric wood shrinkage (S_v) and the volumetric anti-shrink efficiency coefficient (ASE_v) necessary to assess the stabilizing effect of each organosilicon applied.

Volumetric shrinkage (S_v) was calculated according to Eq. (2), where V_0 was the initial volume of a sample immediately after being removed from impregnation solutions, and V_1 was the final volume of a sample (untreated or treated, respectively) after air-drying:

$$S_v = \frac{V_0 - V_1}{V_0} \times 100 \quad (2)$$

Anti-shrink efficiency coefficient (ASE_v) was calculated from the volumetric shrinkage of an untreated (S_{vu}) and a treated sample (S_{vt}) based on Eq. (3):

$$\text{ASE}_v = \frac{S_{vu} - S_{vt}}{S_{vu}} \times 100 \quad (3)$$

Synchrotron-based X-ray fluorescence microscopy (XFM)

XFM was used to map and quantify the infiltration of organosilicon compounds in the wood cell walls of archeological oak wood. Because XFM can simultaneously map multiple elements, the presence of elements between Mg and Zn on the periodic table was also investigated in the archeological wood structure since the presence of some elements (especially Fe and S) can be problematic from the conservation perspective (Fors and Sandström 2006; Lindfors et al. 2008; Broda and Hill 2021; Rémazeilles et al. 2021). The XFM was performed at beamline 2-ID-E at the Advanced Photon Source synchrotron at Argonne National Laboratory in Argonne, IL, USA, following the previously described protocols for wood (Jakes et al. 2015, 2019; Kirker et al. 2017).

For specimen preparation, three small blocks of each treatment with dimensions of about $5 \times 5 \times 8$ mm (radial \times tangential \times longitudinal direction) were cut from previously prepared wood samples and bonded to small steel disks with a 5-min epoxy (Fig. 2). Then, 2- μm -thick transverse wood sections were cut using a Leica EM UC7 ultramicrotome (Wetzlar, Germany) equipped with a diamond knife, placed between two Norcada 200-nm-thick silicon nitride windows (Edmonton, AB, Canada), and mounted on the APS 2-ID-E beamline aluminum stick sample holder. The specimen was tilted 15° toward fluorescence

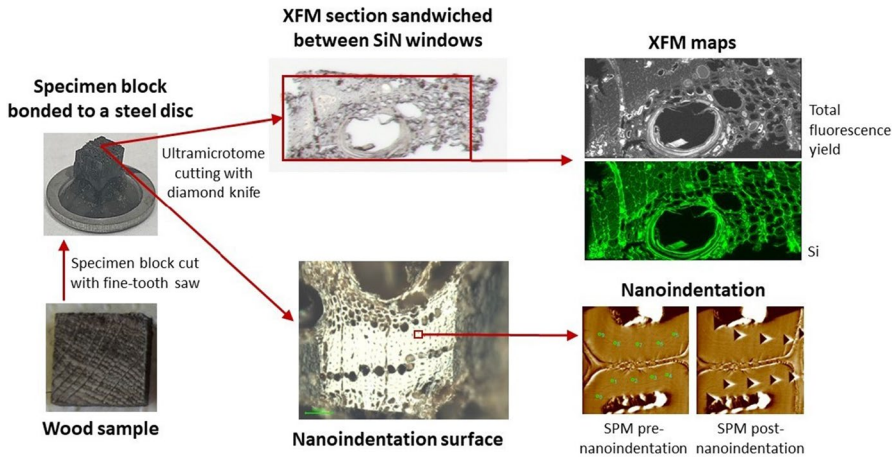


Fig. 2 Experiment scheme including sample preparation for XFM analysis and nanoindentation

detector Vortex[®]-ME4, mounted perpendicular to the incident beam, to reduce the self-absorption effect of fluoresced photons. The beam had incident energy of 10.2 keV and was focused with a zone plate to a spot size of approximately 0.5 μm full width at half maximum (FWHM) in the vertical and 0.6 μm FWHM in the horizontal. Submicron spatial resolution elemental maps were built by a raster scanning the focused X-ray beam across the section using 0.5 μm step sizes and 50 ms dwell time. For each treatment, a total of three sections measuring about 200 μm on a side were mapped, with one section coming from each of the three blocks prepared for each treatment.

The MAPS software package was used to create quantified elemental maps by fitting full spectra to modified Gaussian peaks, iteratively calculating and subtracting the background, and comparing the results to standard reference materials (RF4-100-S1749, AXO DRESDEN GmbH, Heidenau, Germany) (Vogt 2003). Data analysis and Si quantification were performed using the Fiji image processing package (Schindelin et al. 2012) and 32-bit tiff XFM images exported from MAPS. To improve visualization of XFM images, a Gaussian blur (sigma (radius) = 1) filter was applied.

To quantify the amount of Si in the wood cell walls, masks that only contained well-defined cell wall material were manually made using Fiji and XFM maps that clearly displayed the cell walls. The masks were then applied to the Si XFM map to determine the average Si intensity in the cell wall material for each section. The mass of organosilicon that infiltrated the cell wall (organosilicon gain per cell wall volume (OG_{CW})) was calculated using the quantified Si intensity, known section thickness, and organosilicon molecular formula. Estimated cell wall weight percent gain (WPG_{CW}) was also calculated using the mass of organosilicon calculated from XFM analysis and assuming an average value of the cell wall density as 1.45 g cm^{-3} .

Nanoindentation

Nanoindentation was performed in the same wood cells of latewood imaged by XFM by testing the wood cell walls remaining in the wood block after the XFM section was removed (Fig. 2). This allowed a direct comparison between the amount of organosilicon that infiltrated the cell wall and its effect on the cell wall's mechanical properties, similar to previous studies on Br-labeled phenol formaldehyde adhesive infiltration into wood cell walls (Jakes et al. 2015, 2019). After removing the two- μm -thick XFM section, the surface remaining on the block had some knife marks. Ultrasmooth nanoindentation surfaces in the transverse plane were prepared using a Leica EM UC7 ultramicrotome (Wetzlar, Germany) equipped with a diamond knife (Jakes et al. 2008, 2015). The ultrasmooth surface was obtained by removing thinner 200-nm-thick sections from the surface. Nanoindentations were placed on the S2 secondary cell wall layers of the selected cells in the blocks from which the XFM sections were cut. More details about the preparation of nanoindentation surfaces have been described by Jakes and Stone (2021).

A Bruker-Hysitron (Minneapolis, Minnesota, USA) TriboIndenter[®], equipped with a Berkovich probe, was used for the measurements. The machine compliance, probe area function, and tip roundness effects were determined from a series of 80 nanoindentations in a fused silica standard using the load function and procedures described before (Stone et al. 1991; Jakes 2018). Following the calibration reporting procedure prescribed in Jakes (2018): Values for the square root of the Joslin–Oliver parameter of $1.222 \pm 0.002 \mu\text{m}/\text{N}^{1/2}$, the elastic modulus of $71.9 \pm 0.2 \text{ GPa}$, and Meyer's hardness of $9.20 \pm 0.03 \text{ GPa}$ (uncertainties are standard errors) were assessed for fused silica calibration nanoindentations with contact depths between 28 and 193 nm; no systematic variations of machine compliance or Joslin–Oliver parameter were observed in the systematic SYS plot analysis over this range of contact depths.

The relative humidity (RH) inside the nanoindentation enclosure was controlled at $50 \pm 1\%$ RH using an InstruQuest (Coconut Creek, Florida, USA) HumiSysTM HF RH generator. Specimens were conditioned inside the nanoindenter enclosure at least 48 h before experiments, and the RH was maintained during experiments. The temperature inside of the enclosure varied with the laboratory temperature and was measured between 23 and 30 °C during the experiments. The calibration of the temperature and RH sensor inside of the nanoindentation enclosure was verified using a Control Company (Webster, TX, USA) 4085 Traceable[®] Hygrometer Thermometer Dew Point Meter.

The Meyer hardness (H) and nanoindentation elastic modulus (E_s^{NI}) were assessed in the S2 layer using the nanoindentation protocols and analyses given in Jakes and Stone (2021). These protocols and analyses were developed to minimize effects on the H and E_s^{NI} from surface detection errors, structural compliances arising from nearby free edges and cellular flexing (Jakes et al. 2008, 2009), dirty probes, displacement drift, and nanoindenter calibration or performance issues. The multiloading function described in Jakes and Stone (2021) was used in this study with a maximum load of 0.45 mN. Three blocks for each treatment were tested for a total of 12 blocks. In each wood block, at least 20 nanoindentations were placed

in the S2 layer of a minimum of six different fiber cells. The H and E_s^{NI} were calculated for each unloading segment in the multiloading nanoindentations. Then, following established protocols (Jakes and Stone 2021), the H and E_s^{NI} were calculated for each appropriate unloading segment in the multiloading nanoindentations. No data exhibited any systematic size dependence. Therefore, for each treatment, all results from each unloading segment were averaged and used to calculate standard deviations and standard errors.

Results and discussion

The effect of organosilicon treatment on dimensional stability of archeological oak wood

The level of organosilicon impregnation applied on archeological oak wood expressed as bulk wood weight percent gain (WPG_{BW}) is presented in Table 1. Treatment with MTMS had the lowest WPG_{BW} of about 20%, while treatments with MPTMS and DEAPTMS were more effective, reaching the WPG_{BW} values of about 30%. The WPG_{BW} values obtained seem typical for organosilicon treatment of well-preserved archeological oak, resulting from its low permeability (Broda et al. 2019c). For comparison, WPG values for more permeable moderately degraded pine wood were 43%, 58%, and 59% for MTMS, MPTMS, and DEAPTMS, respectively (Broda and Plaza 2023).

Organosilicon retention in the wood structure increased its bulk density from 0.46 g cm^{-3} for untreated samples to about 0.6 g cm^{-3} for treated specimens (Table 1). All these translated into increased dimensional stability of archeological oak during drying. Volumetric wood shrinkage decreased from about 6.5% for untreated wood (Oc) to about 4% for MPTMS-treated samples (O2) and 2.5–2.9% for MTMS- and DEAPTMS-treated ones (O1 and O3, respectively). Based on these results, the highest anti-shrink efficiency was calculated for the treatment with MTMS and DEAPTMS, reaching 55–61%, while for MPTMS, it was only 36% (Table 1). The result obtained for MTMS treatment is in line with our previously reported data for similarly well-preserved waterlogged oak heartwood excavated from the sediments of Lednica Lake, where the anti-shrink efficiency coefficient for MTMS was about 62% (Broda et al. 2019a; c). However, when highly

Table 1 Bulk wood weight percent gain (WPG_{BW}), volumetric shrinkage (S_v), volumetric anti-shrink efficiency (ASE_v), and bulk density (ρ) for archeological oak wood—untreated (Oc), treated with Methyltrimethoxysilane (O1), treated with (3-Mercaptopropyl)trimethoxysilane (O2), and treated with 1,3-Bis-[(diethylamino)-3-(propoxy)propan-2-ol]-1,1,3,3-tetramethyldisiloxane (O3)

Sample	WPG_{BW} (%)	S_v (%)	ASE_v (%)	ρ (g cm^{-3})
Oc	–	6.54 ± 0.39	–	0.46 ± 0.03
O1	22.44 ± 3.10	2.54 ± 1.21	61.20	0.60 ± 0.03
O2	30.66 ± 4.21	4.19 ± 1.38	35.87	0.63 ± 0.02
O3	30.85 ± 2.19	2.92 ± 1.35	55.37	0.59 ± 0.06

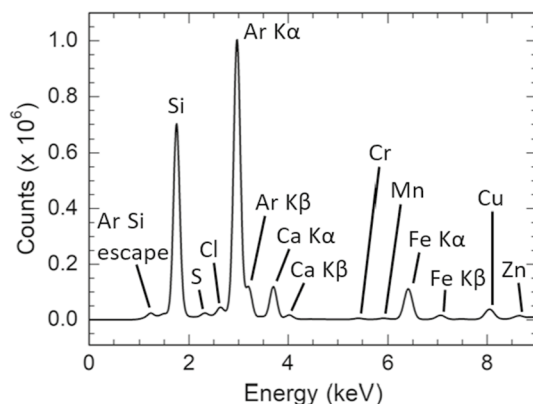
degraded waterlogged elm wood, which had a 48% volumetric shrinking for the control, was treated with MTMS, MPTMS, and DEAPTMS, the highest ASE value was obtained for MPTMS, then DEAPTMS and MTMS reaching 98%, 89.5%, and 80.5%, respectively (Broda et al. 2019b). In this respect, the MPTMS ASE value for oak excavated from the ground that was almost two times lower than that for MTMS or DEAPTMS (Table 1) contradicts results in other types of wood. This suggests that the effectiveness of organosilicons in stabilizing wood dimensions considered as ASE depends not only on the chemical structure of the chemical applied but also on the degree of degradation/anatomical features of the treated wood. On the other hand, when considering this from the performance aspect and the final value of wood shrinkage achieved, the treatments with organosilicons were as or more effective on archeological oak than the highly degraded waterlogged elm.

Mapping of selected elements using an XFM technique

The elements identified from observable peaks in the integral XFM spectra for the untreated archeological oak sample were Si, S, Cl, Ar, Ca, Cr, Mn, Fe, Cu, and Zn (Fig. 3). Argon is a gas that originated from contamination in the air that also produced a Si escape peak (Si is escaping from the detector material itself).

The XFM maps in Fig. 4 reveal the distribution of the elements in an untreated sample. The Ca, Fe, and S are distributed throughout the wood structure and can be used to visualize cellular-scale features like wood secondary cell walls, compound middle lamellae, and lumina. Cl, Cu, Cr, Mn, and Zn are present mainly in localized concentrations or hotspots. Fe ions are visible mainly in the cell lumina and inside ray cells (higher intensity areas in Fig. 4b), with a lesser amount in the cell walls. In turn, Ca and S ions are partly located in the cell lumina and also throughout the secondary cell walls and compound middle lamellae, with higher intensity in the compound middle lamella (Fig. 4a, c). There is likely lower intensity in the secondary cell wall because a substantial volume of the secondary cell wall is occupied by highly ordered cellulose fibrils that are inaccessible to the

Fig. 3 An integral XFM spectral plot identifying individual elements present in a representative untreated oak wood sample



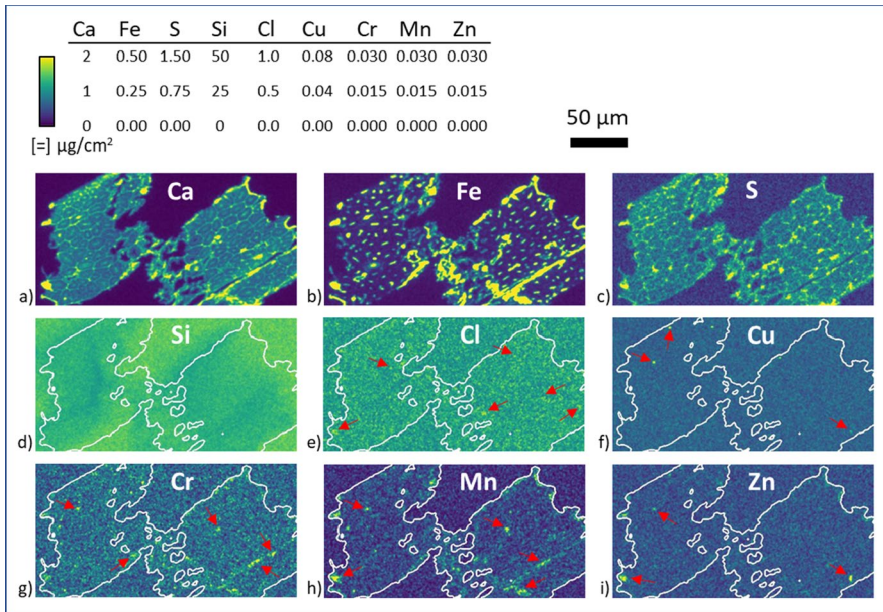


Fig. 4 XFM maps showing localization of the most abundant elements in the untreated archeological oak wood structure: Ca, Fe, S, Cl, Cu, Cr, Mn, and Zn. Outlines in the bottom two rows were obtained from a qualitative thresholding of the Ca map. Arrows point to exemplary hot spots of Cl, Cu, Cr, Mn, and Zn ions in the wood sample

ions. The remaining elements, namely Cl, Cu, Cr, Mn, and Zn, only show up as hot spots inside the wood structure (arrows in Figs. 4e–i, respectively).

Most of the Si signal visible in the maps (Fig. 4d) came from SiN windows used as sample holders in the experiment. The high Si intensity from the SiN window can be observed throughout the map, even in the areas surrounding the sample. There is an expected lower Si intensity where the wood section is (Fig. 4d). The lower Si intensity results from partial absorption by the wood section of the fluoresced photons from the Si in the SiN window behind the wood section. The Si $K\alpha$ fluoresced photon has a 1.84 keV energy. Assuming a two- μm -thick wood cell wall with a density of 1.5 g cm^{-3} and average $\text{C}_4\text{H}_{10}\text{O}_3$ molecular formula, about 15% of the Si $K\alpha$ photons fluoresced from the back window would be expected to be absorbed by the wood section (Henke et al. 1993). Therefore, the observed lower Si intensity was expected for the areas with the wood sections. What was unexpected was that the lower Si intensity was not simply bounded by the outline of the wood section. As observed in Fig. 4d, the Si intensity had a shadow effect in which the intensity was often lower to the left outside of the white section outline. And even within the section outline, the Si intensity was nonuniform. A closer examination of the sandwiched section after XFM revealed that the section was not flat and was still curled. Evidently, the mechanical rigidity of these 200-nm-thick silicon nitride windows was not large enough to completely flatten these sections. We suspect that the shadow effect

and nonuniformity in the Si map were caused by the curl and the 15° angle at which the specimen was held in the beamline.

Calcium and silicon are usually among the most abundant elements in archeological wood excavated from both water bodies and soil (Fors and Sandström 2006; Rémazeilles et al. 2013; Broda and Frankowski 2017; Balzano et al. 2022). Their presence indicates the beginning of the fossilization processes due to the accumulation of mineral compounds such as calcium carbonate (CaCO₃) and silicates (SiO₂) from water that penetrated wood tissue (Schweiggruber and Börner 2018). In our samples, Ca ions are more abundant than Si, which may reflect the local geological characteristics of the place where the wooden remains were discovered, or the smaller particles of silicates were first accumulated and then leached out from wood by groundwater flowing through it.

Iron and sulfur are also commonly found in archeological wood, particularly when waterlogged (Fors and Sandström 2006; Rémazeilles et al. 2013, 2019; Fors et al. 2014; Broda and Frankowski 2017; Björdal and Fors 2019; Balzano et al. 2022). Sulfur is naturally present in various environments and originates from degraded organic matter or compounds released by man (Brown 1982). Except for natural sources and manufactured pollutants, iron associated with wooden archeological artifacts (e.g., shipwrecks or bridge remains) mainly comes from corroding nails, bolts, and other construction elements, as well as from weapons (Fors et al. 2014; Broda and Frankowski 2017; Balzano et al. 2022). Exceptionally high iron concentrations are usually found in archeological oak wood due to the high tannin content. Tannins react with iron and form stable insoluble chemical compounds that accumulate inside the wood and turn its color into black or dark brown (so-called black oak) (Pecoraro et al. 2022; Henrik-Klemens et al. 2022). Waterlogged anoxic conditions rich in sulfur, where waterlogged wooden artifacts are often buried, facilitate the activity of sulfate-reducing bacteria that compete with other anaerobes and facultative anaerobes, including wood-degrading soft-rot and erosion bacteria and produce vast amounts of H₂S (Muyzer and Stams 2008; Björdal and Fors 2019). In the iron-rich environment, H₂S reacts with Fe²⁺ producing various iron sulfides (Monachon et al. 2020), which can crystallize and accumulate in wood, causing further mechanical damage (Wetherall et al. 2008; Balzano et al. 2022). Iron and sulfur compounds can also contribute to the degradation of conservation agents used for archeological wood conservation, such as polyethylene glycol (PEG), causing further wood chemical degradation (Fors and Sandström 2006).

Cl, Cu, Cr, Mn, and Zn ions are usually present in contemporary and archeological wood, resulting from natural environmental processes and human activity, including industrial development (Broda and Frankowski 2017). If they are present in archeological wood in higher concentrations, they can affect the effectiveness of the conservation treatment by decreasing wood permeability.

Si mapping using X-ray fluorescence microscopy

Analysis of Si XFM maps enabled observations of the distribution of organo-silicons within the treated wood structure. As seen in Fig. 5, Fe maps clearly highlighted the cellular wood structure making visualization of features like

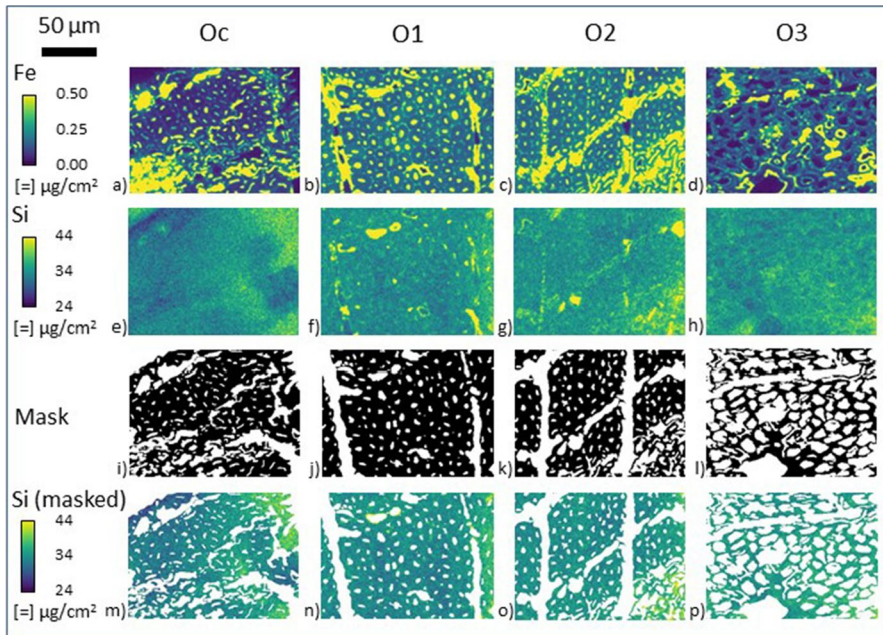


Fig. 5 Representative XFM maps showing localization of Si ions in archeological oak wood – untreated (Oc), treated with Methyltrimethoxysilane (O1), treated with (3-Mercaptopropyl)trimethoxysilane (O2), and treated with 1,3-Bis-[(diethylamino)-3-(propoxy)propan-2-ol]-1,1,3,3-tetramethyldisiloxane (O3). Fe ion maps were included to visualize the wood cell structure

cell walls and lumina possible. In control, MTMS-, and MPTMS-treated sections, most lumina have Fe, which likely suggests these lumina were filled with sediment. Obvious Si hot spots are visible in samples treated with MTMS and MPTMS (Fig. 5f, g, respectively). The hotspots are present in the cell lumina and other open areas in the cellular structure, which indicates that the organosilicons flowed into these wood cavities and likely cured there. Compared to the Fe maps (Fig. 5a–d), it is harder to distinguish the cell walls in the Si maps (Fig. 5e–h). No cell wall features are evident in the Si map of the control sample (Fig. 5e), which suggests that the untreated wood does not have a substantial amount of Si and that the Si signals visible in this map come from a SiN window used as a sample holder in the experiment.

In contrast, cell wall features can be distinguished in Si maps of the organosilicon-treated wood (Fig. 5f–h). This clearly indicates that Si was introduced during treatment and that the treatment process distributed organosilicons throughout the whole wood structure. In the sections with sediment-filled lumina (Fig. 5f, g), the Si intensity seems to be slightly higher in the lumina than the cell walls, suggesting there was more space for the organosilicons to infiltrate the sediment than the cell walls. In the DEAPTMS-treated specimen, which had larger empty lumina, Si intensity is higher in the cell wall than the lumina, which clearly indicates

organosilicon infiltrated the cell walls. Si ions also seem more abundant in visibly more degraded early wood cells (in the bottom right corner in Fig. 5g, h).

From visual observation of XFM maps, it was not possible to conclusively quantify differences in Si content for the different cell walls. To aid in quantification, masks were created (Fig. 5i–l) that only included well-defined cell wall material. Masked Si maps (Fig. 5m–p) enabled the quantification of Si content in cell walls. The results are presented in Table 2 and include the averages of the three sections for each treatment.

An increase in Si content in treated cell walls is evident in the average Si intensity (Table 2), varying between the types of organosilicon compounds used. A few assumptions will need to be made to use these measured intensity increases to quantify the amount of infiltrated organosilicon. The Si intensity increased by 1.5 to 2.1 $\mu\text{g cm}^{-2}$ after treatment. These increases are only a small fraction of the total Si intensity because most of the Si intensity arises from the silicon nitride windows. Therefore, to quantify the organosilicon in the cell wall, it was first assumed that the increase in Si compared to Oc is entirely from the organosilicon in the cell wall. The nonuniformity and shadow effect, as observed in Fig. 4d, also manifested with similar magnitudes of intensity changes. All the sections had similar shadow effects and nonuniformity in their Si maps. The second assumption was that the shadow effect and nonuniformities averaged themselves out over all the specimens, and the observed increases in the treated specimens were from the organosilicon infiltration. The cell wall features distinguished in Si maps of the organosilicon-treated wood (Fig. 5f–h) support that the organosilicon is indeed infiltrating the cell walls, and the quantified Si intensity increases are real.

The Si intensity values were used to calculate organosilicon gain per cell wall volume (OG_{CW}). The highest OG_{CW} of about 0.09 g cm^{-3} was calculated for DEAPTMS-, and the lowest of about 0.04 g cm^{-3} for MTMS-impregnated wood. However, considering the molecular mass of the chemicals used (136.22 g mol^{-1} , 196.34 g mol^{-1} , and 508.88 g mol^{-1} from MTMS, MPTMS, and DEAPTMS,

Table 2 Si signal intensity values, organosilicon gain per cell wall volume (OG_{CW}), estimated cell wall weight percent gain (WPG_{CW}), bulk wood weight percent gain (WPG_{BW}), and the number of organosilicon molecules that infiltrated the cell wall (Mm) of archeological oak wood—untreated (Oc), treated with Methyltrimethoxysilane (O1), treated with (3-Mercaptopropyl)trimethoxysilane (O2), treated with 1,3-Bis-[(diethylamino)-3-(propoxy)propan-2-ol]-1,1,3,3-tetramethyldisiloxane (O3). Standard errors represent the precisions of the measurements and are included to aid in determining differences between samples

Sample	Si intensity ^a ($\mu\text{g cm}^{-2}$)	OG_{CW} ^a (g cm^{-3})	WPG_{CW} ^a (%)	WPG_{BW} ^a (%)	Mm ^a (micromole cm^{-3})
Oc	39.2 ± 0.4	–	–	–	–
O1	40.9 ± 0.8	0.040 ± 0.02	2.7 ± 1.2	22.44 ± 3.10	290 ± 130
O2	40.7 ± 1.0	0.051 ± 0.03	3.5 ± 2.3	30.66 ± 4.21	260 ± 170
O3	41.3 ± 0.8	0.094 ± 0.03	6.5 ± 2.4	30.85 ± 2.19	180 ± 70

^aUncertainties are standard errors

respectively), the highest number of molecules that infiltrated the cell wall was obtained for MTMS-treated wood (290 micromoles per cm^{-3} of the sample), and the lowest for DEAPTMS-treated samples (180 micromoles per cm^{-3}). For MPTMS treatment, it was 260 micromoles per cm^3 .

It is evident that the cell wall weight percent gain (WPG_{CW}) is significantly lower than bulk wood weight percent gain (WPG_{BW}), constituting about 11–12% of its value for MTMS- and MPTS-treated wood and 21% for that DEAPTMS-treated. This indicates that only part of the applied organosilicon compounds infiltrated the well-defined cell walls that were included in the masks. Based on these results and considering the Si maps of treated samples presented in Fig. 5f–h, it can be stated that organosilicon treatment both infiltrated into the cell walls and flowed into lumina, which fits into mixed Norimoto models A2, A3, and A5 (Fig. 1).

For chemical modifications that infiltrate the cell walls, the effect on moisture uptake and swelling is controlled more by the volume of the modifying chemicals deposited in the cell wall (bulking) and not the substitution of the hydroxyl groups by chemical modification (Rowell et al. 1986; Papadopoulos and Hill 2003). In our study, we can observe that the order of magnitudes (i.e., a few percent) of the WPG_{CW} (Table 2) for treated samples is similar to the decrease in wood shrinkage due to the treatment (Table 1). It suggests that the WPG_{CW} gives an indication of how much space in the cell wall the modifying chemical occupies, thereby decreasing the amount of water that can be absorbed. It would be the opposite for shrinkage—in the case of waterlogged wood, the replacement of water molecules by chemicals would prevent wood shrinkage because the chemicals would not evaporate.

Nanoindentation

Nanoindentation enabled the measurement of H and E_s^{NI} of the S2 secondary cell wall layer of untreated and treated archeological oak latewood in the longitudinal direction. From the results presented in Table 3, untreated wood had the lowest E_s^{NI} . The three applied treatments increased the E_s^{NI} of degraded wood by 19%, 21%,

Table 3 Nanoindentation elastic modulus (E_s^{NI}) and hardness (H) results for archeological oak wood—untreated (Oc), treated with Methyltrimethoxysilane (O1), treated with (3-Mercaptopropyl)trimethoxysilane (O2), treated with 1,3-Bis-[(diethylamino)-3-(propoxy)propan-2-ol]-1,1,3,3-tetramethyldisiloxane (O3); N —number of multiloading nanoindentations, n —number of unloading segments analyzed, Std. dev.—standard deviation, Std. er. — standard error

Sample	N	n	E_s^{NI}			H		
			Average (GPa)	Std. dev. (GPa)	Std. er. (GPa)	Average (MPa)	Std. dev. (MPa)	Std. er. (MPa)
Oc	62	536	13.8	3.0	0.1	370	33	1
O1	85	761	16.7	1.8	0.1	388	33	1
O2	80	688	17.6	1.8	0.1	429	26	1
O3	39	273	16.5	1.2	0.1	355	22	1

Standard errors represent the precisions of the measurements and are included to aid in determining differences between samples

and 27% for MTMS, MPTMS, and DEAPTMS, respectively. However, they had a different effect on cell wall H . MTMS, and MPTMS increased H by almost 5% and 16%, respectively, while DEAPTMS reduced cell wall H by about 4%. The changes in cell wall mechanical properties with treatment further support that the applied organosilicons infiltrated the cell walls.

Based on the nanoindentation results, it seems that at least part of the stabilization effect of organosilicons on wood comes from the reinforcement of the cell wall due to its infiltration. However, the highest H obtained for MPTMS treatment does not correlate with its lowest stabilization effect (ASE of only 36% vs. 55% and 61% for the other organosilicons used), which suggests the involvement of some other factors. On the other hand, it should be remembered that the archeological wood used in the study was only slightly degraded (with a loss of wood substance of only about 10%), and although the ASE values were high, the differences in the actual shrinkage between control and treated samples were not very big, ranging of only a few percent (6.5% for control vs. 2.5–4.2% for treated wood).

Regarding the not obvious correlation between improved wood dimensional stability and infiltration and reinforcement of cell walls by organosilicons, it could be hypothesized that filling the cell lumina with the applied chemicals, as seen in Fig. 5f, g, may play a role in stabilizing wood dimensions. For recent undegraded wood treated with various chemicals, it is believed that dimensional stabilization results mainly from cell wall infiltration (bulking) by low-molecular-weight chemicals (plus the formation of polymer network inside the cell wall structure or interactions between chemicals and wood polymers) and that high-molecular-weight ones that cannot penetrate the cell wall and only fill cell lumina only negligibly contribute to dimensional stabilization (Furuno et al. 2004; Ermeydan et al. 2012, 2014; Keplinger et al. 2015; Jakes et al. 2015). However, the conservation treatment of degraded waterlogged archeological wood resulting in dimensional wood stabilization often also involves filling the cell lumina with an applied agent, particularly when high-molecular weight chemicals such as PEG are used (Hoffmann et al. 2004; Bugani et al. 2009; Giachi et al. 2011; Vorobyev et al. 2017; Nguyen et al. 2018). Filling the lumina and other micrometer-sized voids in degraded wood likely prevents the cellular structure from collapsing on itself during drying. Based on these, it can be assumed that the mechanism of archeological wood dimensional stabilization by organosilicon treatment is complex and involves both cell wall infiltration resulting in its reinforcement and filling cell lumina. Since dimensional wood stabilization by organosilicons involves the cell wall infiltration and not necessarily filling the lumina, the weight of the treated wooden artifacts will be lower compared to wood treated with chemicals that fill cell lumina, so its deformation under its own weight will be less likely when displayed in the museum, which is beneficial from the conservation perspective.

It is worth mentioning that the organosilicon infiltration did not plasticize the cell wall substantially. Perhaps it was because of the relatively low WPG due to the low permeability of well-preserved wood, and the effect will increase with much higher WPG that was observed for heavily degraded wood (Broda et al. 2020). Previously

the plasticizing effect of organosilicons was observed in dynamic mechanical analysis (DMA) of bulk specimens (Broda et al. 2021). This method does not address the cell wall properties very well because of the cellular-scale damage in the bulk samples, and the difference between DMA and nanoindentation results concerning plasticizing effect may result from differences in the size scale of the measurement. From this perspective, nanoindentation is needed to actually study the effects of the treatment on wood cell wall material properties.

Conclusion

This research aimed to determine the mechanism of dimensional stabilization of archeological wood by organosilicon compounds using the complementary techniques of synchrotron-based X-ray fluorescence microscopy and nanoindentation.

The combined results of XFM and nanoindentation revealed that part of the organosilicon compounds used for wood treatment infiltrated cell walls enhancing their mechanical properties, and the observed reinforcement of the treated cell wall certainly contributes to dimensional wood stabilization achieved through impregnation with organosilicons. However, because the correlation between the cell wall properties and dimensional stability is not apparent, it indicates the involvement of some other factors like cell wall bulking. XFM results showed that the organosilicon compounds also partially or fully filled some cell lumina, which suggests that organosilicon treatment fits into mixed Norimoto models: A2—infiltration of the cell wall by chemicals, A3—infiltration of the cell wall and partial filling of the cell lumen by chemicals, and A5—both infiltration of the cell wall and complete filling of the lumen by chemicals.

Based on the above and regarding our earlier studies on the interactions between organosilicon compounds and wood polymers, it can be assumed that the mechanism of archeological wood dimensional stabilization by organosilicon treatment is complex and involves chemical interactions between wood and chemicals, and both cell wall infiltration resulting in its reinforcement and filling cell lumina.

Additionally, considering the ASE values and much poorer stabilizing effectiveness of (3-Mercaptopropyl)trimethoxysilane obtained in the study compared to our previous research on severely degraded elm wood, it can be stated that the stabilizing effectiveness of organosilicon compounds depends not only on the chemical structure of the chemical applied but also on the degree of degradation and anatomical features of the treated wood.

Acknowledgements The authors would like to express their thanks to the Directorate of the Poznan Archeological Museum for sharing the historical archeological waterlogged oak piles for research.

Author contributions M.B. and J.E.J. wrote the main manuscript text, prepared all figures, prepared all wood samples and conducted a nanoindentation experiment, L.L. and O.A.A. performed XFM measurements and contributed to the description of the results. All authors reviewed the manuscript.

Funding This research was partially supported by the Polish–U.S. Fulbright Commission through a Fulbright Senior Award 2020/21 granted to Magdalena Broda and funded by the USDA Forest Products Laboratory, Madison, WI, US. Waterlogged wood treatment was supported by the Polish Ministry of Science and Higher Education within the "Cultural heritage—research into innovative solutions and methods

for historic wood conservation" project (No. 2bH 15 0037 83). This research used resources from the Advanced Photon Source, a US Department of Energy (DOE) Office of Science User Facility operated for the DOE Office of Science by Argonne National Laboratory under Contract No. DE-AC02-06CH11357.

Declarations

Conflict of interest On behalf of all authors, the corresponding author states that there is no conflict of interest.

Open Access This article is licensed under a Creative Commons Attribution 4.0 International License, which permits use, sharing, adaptation, distribution and reproduction in any medium or format, as long as you give appropriate credit to the original author(s) and the source, provide a link to the Creative Commons licence, and indicate if changes were made. The images or other third party material in this article are included in the article's Creative Commons licence, unless indicated otherwise in a credit line to the material. If material is not included in the article's Creative Commons licence and your intended use is not permitted by statutory regulation or exceeds the permitted use, you will need to obtain permission directly from the copyright holder. To view a copy of this licence, visit <http://creativecommons.org/licenses/by/4.0/>.

References

- Antonelli F, Galotta G, Sidoti G et al (2020) Cellulose and lignin nano-scale consolidants for waterlogged archaeological wood. *Front Chem* 8:32. <https://doi.org/10.3389/fchem.2020.00032>
- Balzano A, Merela M, Čufar K (2022) Scanning electron microscopy protocol for studying anatomy of highly degraded waterlogged archaeological wood. *Forests* 13:161. <https://doi.org/10.3390/f13020161>
- Björdal CG, Fors Y (2019) Correlation between sulfur accumulation and microbial wood degradation on shipwreck timbers. *Int Biodeterior Biodegrad* 140:37–42. <https://doi.org/10.1016/j.ibiod.2019.03.010>
- Broda M (2018) Biological effectiveness of archaeological oak wood treated with methyltrimethoxysilane and PEG against Brown-rot fungi and moulds. *Int Biodeterior Biodegrad* 134:110–116. <https://doi.org/10.1016/j.ibiod.2018.09.001>
- Broda M, Frankowski M (2017) Determination of the content of selected elements in medieval waterlogged oak wood from the Lednica Lake—a case study. *Environ Sci Pollut R* 24:23401–23410. <https://doi.org/10.1007/s11356-017-9972-7>
- Broda M, Hill CA (2021) Conservation of waterlogged wood—past. Present Future Perspect for 12:1193. <https://doi.org/10.3390/f12091193>
- Broda M, Plaza NZ (2023) Durability of model degraded wood treated with organosilicon compounds against fungal decay. *Int Biodeterior Biodegrad* 178:105562. <https://doi.org/10.1016/j.ibiod.2022.105562>
- Broda M, Popescu C-M (2019) Natural decay of archaeological oak wood versus artificial degradation processes—an FT-IR spectroscopy and X-ray diffraction study. *Spectrochim Acta A-M* 209:280–287. <https://doi.org/10.1016/j.saa.2018.10.057>
- Broda M, Yelle DJ (2022) Reactivity of waterlogged archeological elm wood with organosilicon compounds applied as wood consolidants: 2D 1H–13C solution-state NMR studies. *Molecules* 27:3407. <https://doi.org/10.3390/molecules27113407>
- Broda M, Curling SF, Spear MJ, Hill CAS (2019a) Effect of methyltrimethoxysilane impregnation on the cell wall porosity and water vapour sorption of archaeological waterlogged oak. *Wood Sci Technol* 53:703–726. <https://doi.org/10.1007/s00226-019-01095-y>
- Broda M, Mazela B, Dutkiewicz A (2019b) Organosilicon compounds with various active groups as consolidants for the preservation of waterlogged archaeological wood. *J Cult Herit* 35:123–128. <https://doi.org/10.1016/j.culher.2018.06.006>
- Broda M, Mazela B, Radka K (2019c) Methyltrimethoxysilane as a stabilising agent for archaeological waterlogged wood differing in the degree of degradation. *J Cult Herit* 35:129–139. <https://doi.org/10.1016/j.culher.2018.06.004>

- Broda M, Dąbek I, Dutkiewicz A et al (2020) Organosilicons of different molecular size and chemical structure as consolidants for waterlogged archaeological wood—a new reversible and retreatable method. *Sci Rep* 10:1–13. <https://doi.org/10.1038/s41598-020-59240-8>
- Broda M, Spear MJ, Curling SF, Ormondroyd GA (2021) The viscoelastic behaviour of waterlogged archaeological wood treated with methyltrimethoxysilane. *Materials* 14:5150. <https://doi.org/10.3390/ma14185150>
- Broda M, Spear MJ, Curling SF, Dimitriou A (2022) Effects of biological and chemical degradation on the properties of scots pine—part II: wood-moisture relations and viscoelastic behaviour. *Forests* 13:1390. <https://doi.org/10.3390/f13091390>
- Brown KA (1982) Sulphur in the environment: a review. *Environ Pollut B* 3:47–80. [https://doi.org/10.1016/0143-148X\(82\)90042-8](https://doi.org/10.1016/0143-148X(82)90042-8)
- Bugani S, Modugno F, Lucejko JJ et al (2009) Study on the impregnation of archaeological waterlogged wood with consolidation treatments using synchrotron radiation microtomography. *Anal Bioanal Chem* 395:1977–1985. <https://doi.org/10.1007/s00216-009-3101-5>
- Cavallaro G, Lazzara G, Milioto S et al (2017) Nanocomposites based on esterified colophony and halloysite clay nanotubes as consolidants for waterlogged archaeological woods. *Cellulose* 24:3367–3376. <https://doi.org/10.1007/s10570-017-1369-8>
- Christensen M, Larnøy E, Kutzke H, Hansen FK (2015) Treatment of waterlogged archaeological wood using chitosan and modified chitosan solutions. Part 1: chemical compatibility and microstructure. *J Am Inst Conserv* 54:3–13. <https://doi.org/10.1179/1945233014Y.0000000034>
- Ermeidan MA, Cabane E, Masic A et al (2012) Flavonoid insertion into cell walls improves wood properties. *ACS Appl Mater Interfaces* 4:5782–5789. <https://doi.org/10.1021/am301266k>
- Ermeidan MA, Cabane E, Gierlinger N et al (2014) Improvement of wood material properties via in situ polymerization of styrene into tosylated cell walls. *RSC Adv* 4:12981–12988. <https://doi.org/10.1039/C4RA00741G>
- Fors Y, Sandström M (2006) Sulfur and iron in shipwrecks cause conservation concerns. *Chem Soc Rev* 35:399–415. <https://doi.org/10.1039/B507010B>
- Fors Y, Grudd H, Rindby A et al (2014) Sulfur and iron accumulation in three marine-archaeological shipwrecks in the Baltic Sea: the ghost, the crown and the sword. *Sci Rep* 4:4222. <https://doi.org/10.1038/srep04222>
- Furuno T, Imamura Y, Kajita H (2004) The modification of wood by treatment with low molecular weight phenol-formaldehyde resin: a properties enhancement with neutralized phenolic-resin and resin penetration into wood cell walls. *Wood Sci Technol* 37:349–361. <https://doi.org/10.1007/s00226-003-0176-6>
- Giachi G, Capretti C, Donato ID et al (2011) New trials in the consolidation of waterlogged archaeological wood with different acetone-carried products. *J Archaeol Sci* 38:2957–2967. <https://doi.org/10.1016/j.jas.2011.06.012>
- Grattan DW (1987) 3 - Waterlogged wood. In: Pearson C (ed) Conservation of marine archaeological objects. Butterworth-Heinemann, Oxford, pp 55–67
- Guo J, Xiao L, Han L et al (2019) Deterioration of the cell wall in waterlogged wooden archeological artifacts, 2400 years old. *IAWA J* 40:820–844. <https://doi.org/10.1163/22941932-40190241>
- Guo J, Chen J, Li R et al (2022) Thermoporometry of waterlogged archaeological wood: insights into the change of pore traits after the water-removal by supercritical drying. *Thermochim Acta* 715:179297. <https://doi.org/10.1016/j.tca.2022.179297>
- Han L, Tian X, Keplinger T et al (2020) Even visually intact cell walls in waterlogged archaeological wood are chemically deteriorated and mechanically fragile: a case of a 170 year-old shipwreck. *Molecules* 25:1113. <https://doi.org/10.3390/molecules25051113>
- Henke BL, Gullikson EM, Davis JC (1993) X-ray interactions: photoabsorption, scattering, transmission, and reflection at $E = 50\text{--}30,000$ eV, $Z = 1\text{--}92$. *At Data Nucl Data Tables* 54:181–342. <https://doi.org/10.1006/adnd.1993.1013>
- Henrik-Klemens Å, Bengtsson F, Björdal CG (2022) Raman spectroscopic investigation of iron-tannin precipitates in waterlogged archaeological oak. *Stud Conserv* 67:237–247. <https://doi.org/10.1080/00393630.2020.1864895>
- Hoffmann P, Singh A, Kim YS et al (2004) The Bremen Cog of 1380—an electron microscopic study of its degraded wood before and after stabilization with PEG. *Holzforschung* 58:211–218. <https://doi.org/10.1515/HF.2004.033>
- Jakes JE (2018) Improved methods for nanoindentation Berkovich probe calibrations using fused silica. *J Mater Sci* 53:4814–4827. <https://doi.org/10.1007/s10853-017-1922-8>

- Jakes JE, Stone DS (2021) Best practices for quasistatic Berkovich nanoindentation of wood cell walls. *Forests* 12:1696. <https://doi.org/10.3390/f12121696>
- Jakes JE, Frihart CR, Beecher JF et al (2008) Experimental method to account for structural compliance in nanoindentation measurements. *J Mater Res* 23:1113–1127. <https://doi.org/10.1557/jmr.2008.0131>
- Jakes JE, Frihart CR, Beecher JF et al (2009) Nanoindentation near the edge. *J Mater Res* 24:1016–1031. <https://doi.org/10.1557/jmr.2009.0076>
- Jakes JE, Hunt CG, Yelle DJ et al (2015) Synchrotron-based X-ray fluorescence microscopy in conjunction with nanoindentation to study molecular-scale interactions of phenol-formaldehyde in wood cell walls. *ACS Appl Mater Interfaces* 7:6584–6589. <https://doi.org/10.1021/am5087598>
- Jakes JE, Frihart CR, Hunt CG et al (2019) X-ray methods to observe and quantify adhesive penetration into wood. *J Mater Sci* 54:705–718. <https://doi.org/10.1007/s10853-018-2783-5>
- Jakes JE, Zelinka SL, Hunt CG et al (2020) Measurement of moisture-dependent ion diffusion constants in wood cell wall layers using time-lapse micro X-ray fluorescence microscopy. *Sci Rep* 10:9919. <https://doi.org/10.1038/s41598-020-66916-8>
- Kaye B (1995) Conservation of waterlogged archaeological wood. *Chem Soc Rev* 24:35–43. <https://doi.org/10.1039/CS9952400035>
- Keplinger T, Cabane E, Chanana M et al (2015) A versatile strategy for grafting polymers to wood cell walls. *Acta Biomater* 11:256–263. <https://doi.org/10.1016/j.actbio.2014.09.016>
- Kirker G, Zelinka S, Glexer S-C et al (2017) Synchrotron-based X-ray fluorescence microscopy enables multiscale spatial visualization of ions involved in fungal lignocellulose deconstruction. *Sci Rep* 7:41798. <https://doi.org/10.1038/srep41798>
- Kowalczyk J, Rachocki A, Broda M et al (2019) Conservation process of archaeological waterlogged wood studied by spectroscopy and gradient NMR methods. *Wood Sci Technol* 53:1207–1222. <https://doi.org/10.1007/s00226-019-01129-5>
- Lindfors E-L, Lindström M, Iversen T (2008) Polysaccharide degradation in waterlogged oak wood from the ancient warship Vasa. *Holzforschung* 62:57–63. <https://doi.org/10.1515/HF.2008.008>
- Lisuzzo L, Hueckel T, Cavallaro G et al (2021) Pickering emulsions based on wax and halloysite nanotubes: an ecofriendly protocol for the treatment of archeological woods. *ACS Appl Mater Interfaces* 13:1651–1661. <https://doi.org/10.1021/acsami.0c20443>
- McHale E, Braovac S, Steindal CC et al (2016) Synthesis and characterisation of lignin-like oligomers as a bio-inspired consolidant for waterlogged archaeological wood. *Pure Appl Chem* 88:969–977. <https://doi.org/10.1515/pac-2016-0814>
- McHale E, Steindal CC, Kutzke H et al (2017) In situ polymerisation of isoeugenol as a green consolidation method for waterlogged archaeological wood. *Sci Rep* 7:46481. <https://doi.org/10.1038/srep46481>
- Monachon M, Albelda-Berenguer M, Pelé C et al (2020) Characterization of model samples simulating degradation processes induced by iron and sulfur species on waterlogged wood. *Microchem J* 155:104756. <https://doi.org/10.1016/j.microc.2020.104756>
- Muyzer G, Stams AJM (2008) The ecology and biotechnology of sulphate-reducing bacteria. *Nat Rev Microbiol* 6:441–454. <https://doi.org/10.1038/nrmicro1892>
- Nguyen TD, Kohdzuma Y, Endo R, Sugiyama J (2018) Evaluation of chemical treatments on dimensional stabilization of archeological waterlogged hardwoods obtained from the Thang Long Imperial Citadel site, Vietnam. *J Wood Sci* 64:436–443. <https://doi.org/10.1007/s10086-018-1719-7>
- Norimoto M (2001) Chemical modification of wood. In: Hon DN-S, Shirashi N (eds) *Wood and cellulose chemistry*, 2nd edn. Marcel Dekker, New York, pp 573–598
- Osterholtz FD, Pohl ER (1992) Kinetics of the hydrolysis and condensation of organofunctional alkoxy-silanes: a review. *J Adhes Sci Technol* 6:127–149. <https://doi.org/10.1163/156856192X00106>
- Papacchini A, Dominici S, Di Giulio G et al (2019) Bio-based consolidants for waterlogged archaeological wood: assessment of the performance and optimization of the diagnostic protocol. *J Cult Herit* 40:49–58. <https://doi.org/10.1016/j.culher.2019.05.009>
- Papadopoulos AN, Hill CAS (2003) The sorption of water vapour by anhydride modified softwood. *Wood Sci Technol* 37:221–231. <https://doi.org/10.1007/s00226-003-0192-6>
- Parisi F, Bernardini F, Cavallaro G et al (2020) Halloysite nanotubes/pluronic nanocomposites for waterlogged archaeological wood: thermal stability and X-ray microtomography. *J Therm Anal Calorim* 141:981–989. <https://doi.org/10.1007/s10973-020-09637-4>
- Paunesku T, Vogt S, Maser J et al (2006) X-ray fluorescence microprobe imaging in biology and medicine. *J Cell Biochem* 99:1489–1502. <https://doi.org/10.1002/jcb.21047>

- Pecoraro E, Pelé-Meziani C, Macchioni N et al (2022) The removal of iron from waterlogged archaeological wood: efficacy and effects on the room temperature wood properties. *Wood Mater Sci Eng*. <https://doi.org/10.1080/17480272.2022.2061870>
- Pizzo B, Pecoraro E, Lazzeri S (2018) Dynamic mechanical analysis (DMA) of waterlogged archaeological wood at room temperature. *Holzforschung* 72:421–431. <https://doi.org/10.1515/hf-2017-0114>
- Popescu C-M, Broda M (2021) Interactions between different organosilicons and archaeological waterlogged wood evaluated by infrared spectroscopy. *Forests* 12:268. <https://doi.org/10.3390/f12030268>
- Rémazeilles C, Tran K, Guilminot E et al (2013) Study of Fe(II) sulphides in waterlogged archaeological wood. *Stud Conserv* 58:297–307. <https://doi.org/10.1179/2047058412Y.0000000071>
- Rémazeilles C, Lévêque F, Conforto E et al (2019) Contribution of magnetic measurement methods to the analysis of iron sulfides in archaeological waterlogged wood-iron assemblies. *Microchem J* 148:10–20. <https://doi.org/10.1016/j.micro.2019.04.062>
- Rémazeilles C, Lévêque F, Conforto E, Refait P (2021) Long-term alteration processes of iron fasteners extracted from archaeological shipwrecks aged in biologically active waterlogged media. *Corros Sci* 181:109231. <https://doi.org/10.1016/j.corsci.2020.109231>
- Rowell RM, Tillman A-M, Zhengtian L (1986) Dimensional stabilization of flakeboard by chemical modification. *Wood Sci Technol* 20:83–95. <https://doi.org/10.1007/BF00350696>
- Schindelin J, Arganda-Carreras I, Frise E et al (2012) Fiji: an open-source platform for biological-image analysis. *Nat Methods* 9:676–682. <https://doi.org/10.1038/nmeth.2019>
- Schweingruber FH, Börner A (2018) Fossilization, permineralization, coalification, carbonization and wet wood conservation. In: Schweingruber FH, Börner A (eds) *The plant stem: a microscopic aspect*. Springer International Publishing, Cham, pp 183–192
- Spear MJ, Broda M (2020) Comparison of contemporary elm (*Ulmus* spp.) and degraded archaeological elm: the use of dynamic mechanical analysis under ambient moisture conditions. *Materials* 13:5026. <https://doi.org/10.3390/ma13215026>
- Stempin A (2018) The early Piast settlement on Ostrów Tumski (Cathedral Island) in Poznań—the popularisation of heritage from the standpoint of the genius loci archaeological reserve. *Analecta Archaeol Ressorviensia* 13:275–286
- Stone DS, Yoder KB, Sproul WD (1991) Hardness and elastic modulus of TiN based on continuous indentation technique and new correlation. *J Vac Sci Technol* 9:2543–2547. <https://doi.org/10.1116/1.577270>
- Svedström K, Bjurhager I, Kallonen A et al (2012) Structure of oak wood from the Swedish warship Vasa revealed by X-ray scattering and microtomography. *Holzforschung* 66:355–363. <https://doi.org/10.1515/hf.2011.157>
- Unger A, Schniewind A, Unger W (2001) *Conservation of wood artifacts: a handbook*. Springer Science & Business Media, Cham
- Vogt S (2003) MAPS: a set of software tools for analysis and visualization of 3D X-ray fluorescence data sets. *J Phys IV Fr* 104:635–638. <https://doi.org/10.1051/jp4:20030160>
- Vorobyev A, Almkvist G, van Dijk NP, Gamstedt EK (2017) Relations of density, polyethylene glycol treatment and moisture content with stiffness properties of Vasa oak samples. *Holzforschung* 71:327–335. <https://doi.org/10.1515/hf-2016-0202>
- Wakefield JM, Hampe R, Gillis RB et al (2020) Aminoethyl substitution enhances the self-assembly properties of an aminocellulose as a potential archaeological wood consolidant. *Eur Biophys J* 49:791–798. <https://doi.org/10.1007/s00249-020-01451-y>
- Walsh-Korb Z, Stelzner I, dos Santos GJ et al (2022) Morphological study of bio-based polymers in the consolidation of waterlogged wooden objects. *Materials* 15:681. <https://doi.org/10.3390/ma15020681>
- Wetherall KM, Moss RM, Jones AM et al (2008) Sulfur and iron speciation in recently recovered timbers of the Mary Rose revealed via X-ray absorption spectroscopy. *J Archaeol Sci* 35:1317–1328. <https://doi.org/10.1016/j.jas.2007.09.007>
- Wimmer R, Lucas BN, Oliver WC, Tsui TY (1997) Longitudinal hardness and Young's modulus of spruce tracheid secondary walls using nanoindentation technique. *Wood Sci Technol* 31:131–141. <https://doi.org/10.1007/BF00705928>
- Xia Y, Chen T-Y, Wen J-L et al (2018) Multi-analysis of chemical transformations of lignin macromolecules from waterlogged archaeological wood. *Int J Biol Macromol* 109:407–416. <https://doi.org/10.1016/j.ijbiomac.2017.12.114>
- Zhou Y, Wang K, Hu D (2019) High retreatability and dimensional stability of polymer grafted waterlogged archaeological wood achieved by ARGET ATRP. *Sci Rep* 9:1–9. <https://doi.org/10.1038/s41598-019-46366-7>

Publisher's Note Springer Nature remains neutral with regard to jurisdictional claims in published maps and institutional affiliations.